JOURNAL OF MATERIALS SCIENCE 21 (1986) 3668–3672

Effect of crystallinity in the thermal behaviour of nickel hydroxide

J. M. FERNÁNDEZ RODRÍGUEZ, J. MORALES, J. L. TIRADO
Departamento de Química Inorgánica, Facultad de Ciencias, Universidad de Córdoba, Córdoba, Spain

The textural and structural characteristics of nickel hydroxide condition the properties of its thermal decomposition product. The thermal behaviour is also affected. Thus, the differential scanning calorimetry traces of a sample of low crystallinity shows an exothermal peak which is indicative of a process of release of the energy stored as defects. This interpretation is evidenced by a loss of microstrains in the temperature interval of the exotherm.

1. Introduction

The characterization of the $Ni(OH)_2$–NiO system has been developed in depth in recent years [1–5]. However, the constant interest on this system is evidenced by recent reports on some new aspects concerning the preparation [6], thermal behaviour [7] and structural properties [8] of these phases.

The thermal dehydration of $Ni(OH)_2$ yields NiO, with the development of an endothermal effect in the differential thermal analysis (DTA) traces of this material. This effect is only usually recognized in the curves of $Ni(OH)_2$. In a recent article, new emphasis has been made on a low-area exothermal effect present in some DTA traces of the hydroxide immediately after dehydration [9]. This effect has been explained in terms of an amorphous-to-crystalline transformation, in contrast with previous interpretations based on a rhombohedral–cubic transition of NiO [10]. However definitive data to support these interpretations have not been reported.

On the other hand, the effect of the method used in sample preparation has not been taken into account in the interpretation of the thermal behaviour of $Ni(OH)_2$. In this respect, previous reports [11] did not notice the above mentioned exotherm in well-crystallized and turbostratic samples, probably indicating that the textural and structural characteristics of the parent solid have major effects on the thermal behaviour of NiO. Additionally, it has been recently shown [12] that the surface properties of NiO depend markedly on the conditions in which the thermal decomposition of $Ni(OH)_2$ is carried out.

The aim of this article is to examine the thermal evolution of the characteristics of NiO derived from two samples of $Ni(OH)_2$ of different texture and crystallinity, in order to give a new light on the thermal effects shown in their DTA and differential scanning calorimetry (DSC) traces.

2. Experimental details

Three samples of nickel hydroxide were prepared: sample A was obtained by adding 0.1 M NaOH to a 0.1 M solution of $Ni(NO_3)_2$. The precipitate was suspended in water three times to eliminate sodium ions. Sample B was prepared by passing ammonia through the same $Ni(NO_3)_2$ solution at 25° C and ageing the precipitate by allowing it to be suspended in water for 90 days. A third sample, henceforth referred to as C, was prepared from sample A by hydrothermal treatment in a laboratory autoclave Berghof at 200° C for 6 days. The X-ray diffraction patterns of these samples showed reflections of β-$Ni(OH)_2$ exclusively, although a different broadening of the lines was observed in each case, as discussed below.

The DSC diagrams were obtained with a Mettler TA3000 apparatus, provided with a TC 10 TA processor unit. The calibration was carried out with an indium metal sample. The DSC equipment was also used to prepare decomposed samples from A, B and C at fixed temperatures. The experiments were always performed in static air atmosphere, at a heating rate of $8°\,C\,min^{-1}$ and sample weights of ~ 50 mg.

The isotherms of nitrogen adsorption at 77 K were determined in a pyrex high vacuum apparatus, and the dead space was calibrated with helium gas. Pressures were read by a digital manometer Balzers APR-010 to an accuracy of 0.1 mbar. The data were processed by a computer program described in [13].

Powder X-ray diffraction patterns were obtained with a Philips PW1130 diffractometer using Co$K\alpha$ radiation and an iron filter. The profiles used in line broadening analysis were recorded at $0.125°\,min^{-1}$ and the intensities were read each $0.025°\,2\theta$. The computation of the values of crystallite size and microstrains content was carried out by two alternative methods: from the integral breadth and full width at half maximum (FWHM) by profile fitting to a Pearson VII function [14]. From the cosine Fourier coefficients of the f profiles, by the method described in [15]. The instrumental g profiles used in the analysis of the 0 0 1 and 1 1 0 lines of $Ni(OH)_2$ were the 1 1 1 and 4 2 0 lines of a recrystallized sample of lead nitrate. For NiO, a sample of this oxide annealed at 1100° C for 5 h was used to obtain the g profiles.

Transmission electron micrographs were obtained with a Philips EM 300 apparatus. Samples were

0022–2461/86 $03.00 + .12

TABLE I Results of the X-ray diffraction line profile analysis

h k l	Sample	Profile fitting to P-VII		Single-line Fourier	
		ε_β*	$\tilde{e}$†	ε_F*	$(\langle e^2\rangle)^{1/2}$†
	A	116	86.2	20	70.1
0 0 1	B	288	10.0	105	13.1
	C	826	3.3	347	6.4
	A	251	5.0	59	5.7
1 1 0	B	537	0.7	554	1.6
	C		–	960	1.5
	A310	130	29.0	54	16.4
1 1 1	B370	109	10.4	49	5.3
	C340	126	5.0	70	9.1
	A310	104	6.9	73	8.5
2 2 0	B370	137	8.6	84	8.6
	C340	196	6.5	87	7.5
1 1 1	A370	121	18.7	53	8.9
1 1 1	B430	154	10.3	59	4.9

*$\varepsilon_{\beta,F}$: Volume-averaged and area-averaged crystallite size (A).
†$\tilde{e}$, $(\langle e^2\rangle)^{1/2}$: Microstains 10^3.

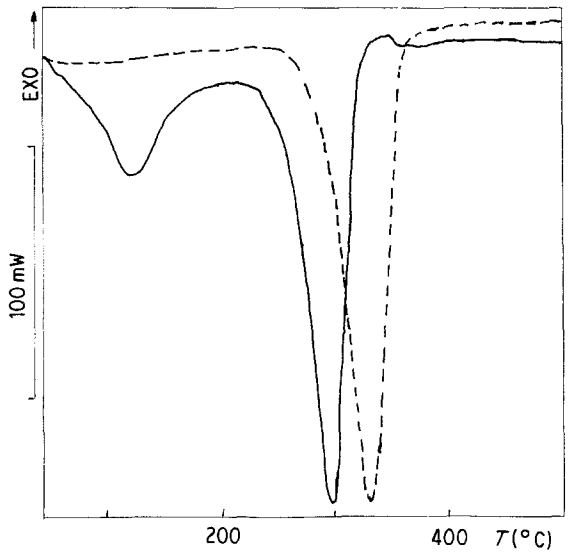

Figure 1 DSC traces of sample A (poorly crystalline $Ni(OH)_2$) and B (well crystallized nickel hydroxide). (—) A; (– – –) B.

dispersed in acetone by ultrasound and placed on copper grids covered with a carbon film for their examination.

3. Results and discussion

The average values of crystallite size and microstrains content were evaluated in samples A, B and C of nickel hydroxide by the analysis of the X-ray line profiles of the 0 0 1 and 1 1 0 reflections of β-$Ni(OH)_2$ (see Table I). The comparison of the results obtained by profile fitting and Fourier procedures is in good agreement with the different definition of the structural parameters in each case [14]. On the other hand, a differential broadening was observed in the studied lines that leads to different values of the structural parameters in each crystallographic direction. This accounts for a lower value of crystallite size in the [0 0 1] direction, which is consistent with the plate-like shape of the particles of the hydroxide, also adopted by the coherently diffracting domains [16].

Other facts of interest from the results in Table I are a content of microstrains which is higher for lower sized crystallites and for the 0 0 1 direction. Additionally, it should be emphasized that despite the different crystallinity of each sample, they showed all *h k l* reflections. This should be interpreted by considering that for the A sample the low values of ε_β and ε_F in the 0 0 1 line means thin plates but not a random stacking of plates as in turbostratic nickel hydroxide [17].

The characteristics of crystallinity of each sample condition the values of the structural parameters of the NiO samples resulting from their thermal decomposition. Table I also shows the values of crystallite size and microstrains for oxide samples obtained by interrupting DSC experiments at a temperature in which the parent hydroxide is completely decomposed. These were calculated for the crystallographic directions in which the hydroxide 0 0 1 and 1 1 0 transform topotactically [1]. Several comments should be made to these data. First it is noteworthy that the differences in the values of crystallite size for different samples and reflections are not so notorious as in the case of the parent samples. This fact is in agreement with the pseudocubic structure of NiO [4] that may condition a more isotropic shape of coherently diffracting domains. On the contrary, the content of microstrains in the [1 1 1] direction reveals a direct influence of the distortions in the parent hydroxide. For the 2 2 0 reflection, the similarity in $\tilde{e}$ and $(\langle e^2\rangle)^{1/2}$ may be due to the lower content in the [1 1 0] direction of $Ni(OH)_2$.

Fig. 1 shows the DSC diagrams of samples A and B. The diagram for sample C was similar to that of the $Ni(OH)_2$ sample prepared with ammonia. It is worthy to note that both traces show significant divergences. Thus, the A sample shows a broad, low-temperature endotherm caused by the loss of weakly bound water which is absent for the B sample. Additionally, the dehydroxylation peak develops at lower temperatures for the sample prepared with NaOH. But the most relevant feature in these diagrams is the occurrence of a small exothermal peak for sample A. This peak is in principle independent of the base used in the precipitation reaction, as the effect is absent for both B and C samples.

The nature of the exothermal peak was studied by first considering the interpretations previously proposed. The possibility that a rhombohedral–cubic transition [10] could be responsible of the evolved heat is not in principle immediate, as recent studies on NiO have shown [2, 18] that the structure of this oxide is rhombohedral in a broad temperature interval with continuous changes in the pseudo-cubic parameter *a* on heating. A second explanation based in an amorphous to crystalline transition [9] is not evident from the fact that partially decomposed samples, as those shown in Fig. 2 show reflections of $Ni(OH)_2$ and NiO simultaneously, discarding the existence of an amorphous intermediate.

On the other hand, analogous thermal effects placed immediately after the dehydration of hydroxycompounds have been interpreted in terms of a surface reordering process that causes an energy release [19, 20]. This possibility was also considered for

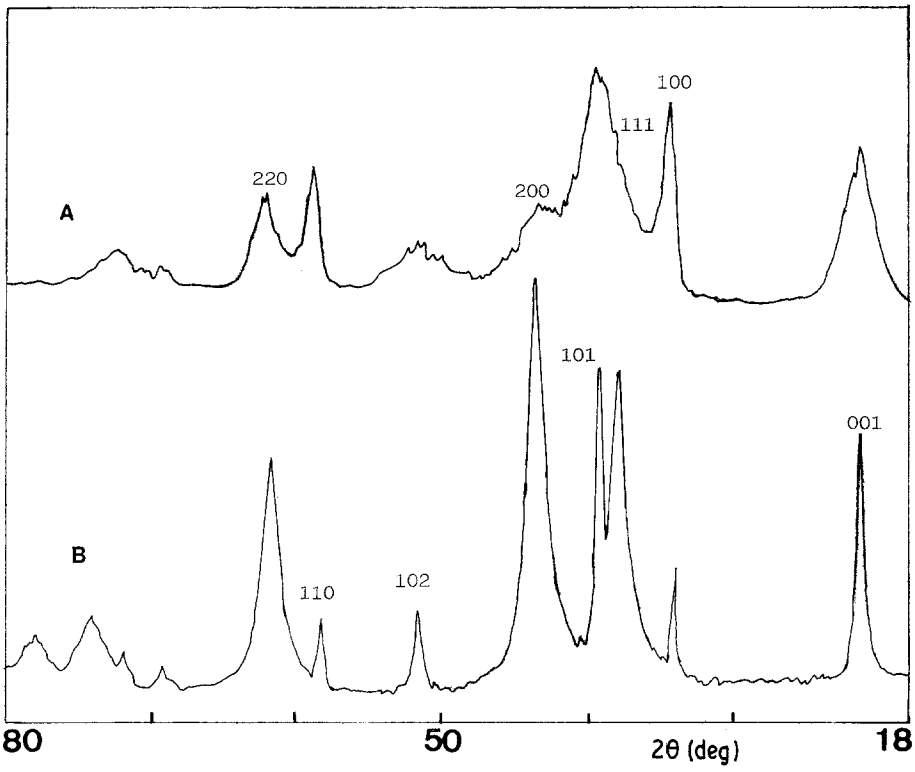

Figure 2 X-ray diffraction patterns of partially decomposed samples of $Ni(OH)_2$. The Miller indices of NiO lines are shown for sample A and those of β-$Ni(OH)_2$ for sample B.

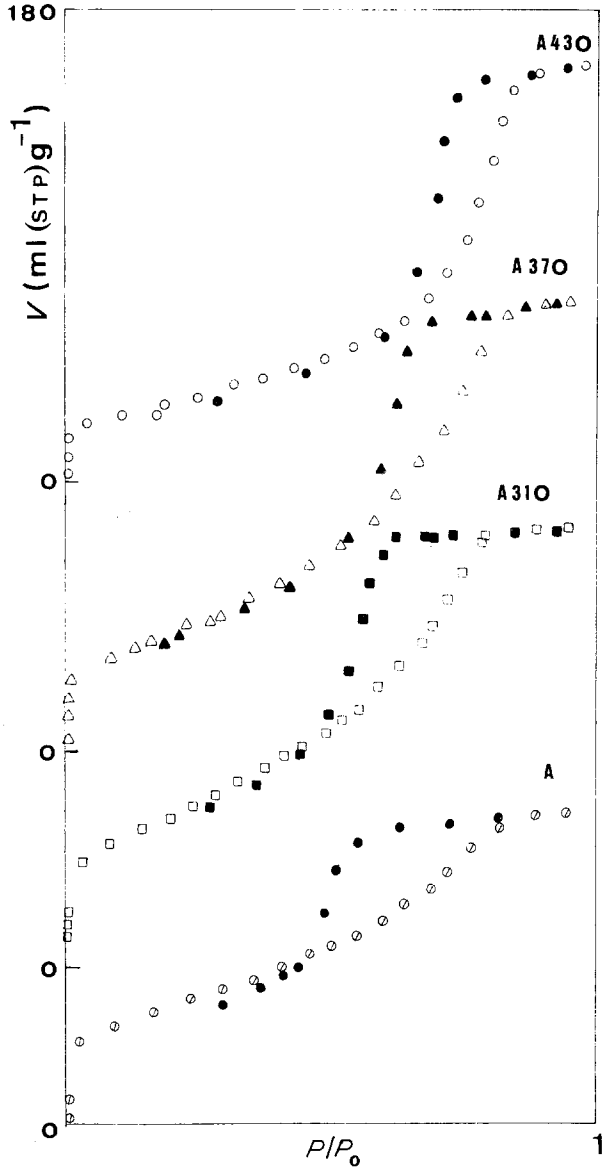

Figure 3 Nitrogen adsorption isotherms for sample A after thermal treatment at different temperatures.

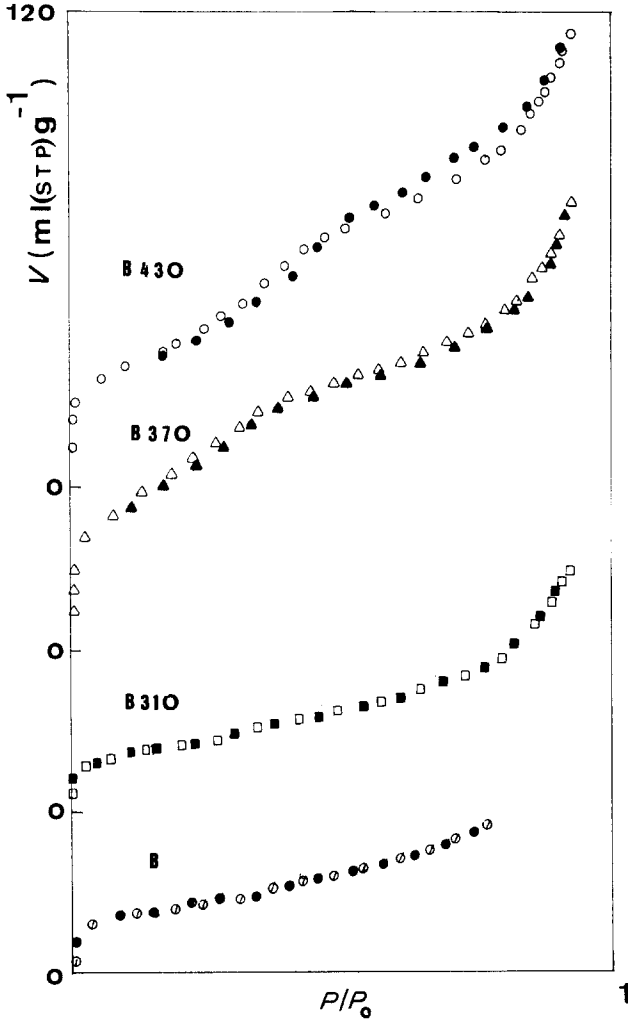

Figure 4 Nitrogen adsorption isotherms for sample B after thermal treatment at different temperatures.

TABLE II Results of the analysis of gas adsorption measurements

Sample	S_{BET} ($m^2 g^{-1}$)	C_{BET}	V_p (ml (liq) g^{-1})
A	164.7	130	0.188
A310	211.1	83	0.263
A370	174.9	43	0.269
A430	107.9	55	0.243
B	62.0	55	
B310	57.9	55	
B370	183.9	33	
B430	141.5	36	

the $Ni(OH)_2$ case. In this way, Figs 3 and 4 show the adsorption–desorption isotherms for different samples obtained by interrupting the DSC experiment at selected temperatures. First it is noticeable that the two series of samples have a characteristic behaviour, reflected in the shape and reversibility of the isotherms. This divergence may be connected with the different adsorption behaviour of the parent A and B samples. While the B sample shows a typical type II isotherm, according to the BDDT classification, the A sample shows an adsorption sequence commonly found in microporous solids [21]. The differences between the adsorption and desorption branches may be related to pore interconnectivity phenomena [22].

The effect of the thermal treatment on the adsorption isotherms is also relevant. For the A samples, the shape of the isotherm alters slightly between 310 and 430° C by a progressive displacement of the low-pressure point of closure of the hysteresis loop, indicating an increase in pore size. Instead, the B samples show a characteristic shape at temperatures above the decomposition (B370 and B430). These curves consist of a type II with an inflection point, in good agreement with previous reports [1]. It should be noted that the second pattern is only obtained for well crystallized samples decomposed in air atmosphere. A recent study [12] showed a different behaviour for the products of the thermal decomposition of this sample in vacuum for temperatures below 500° C.

Additional information was obtained by the analysis of the adsorption branches of the isotherms by the BET method (Table II). These results show that the decomposition process (A310 and B370) takes place with a considerable increase in specific surface, behaviour commonly found in other dehydroxylation processes. For the A sample, this change is accompanied by a significant increase in the values of pore volume (V_p) computed from the intercept of the horizontal branch of the isotherm. From the decomposition temperature, a gradual loss of BET surface is observed independently of the parent sample. The slight variation found before (A310 and B370) and after the exothermal effect (A370 and B430) allows not to assign the exotherm to the energy released in a surface reordering process.

The electron micrographs in Fig. 5 are in correspondence with the adsorption data. Thus, the undecomposed samples show marked differences that condition the texture of the oxide derived in each case. The presence of a porous system in A samples may be connected with the interparticle space. Between 310 and 370° C no significant change is observed in the texture of the samples derived from A.

From the results in Table I, an alternative

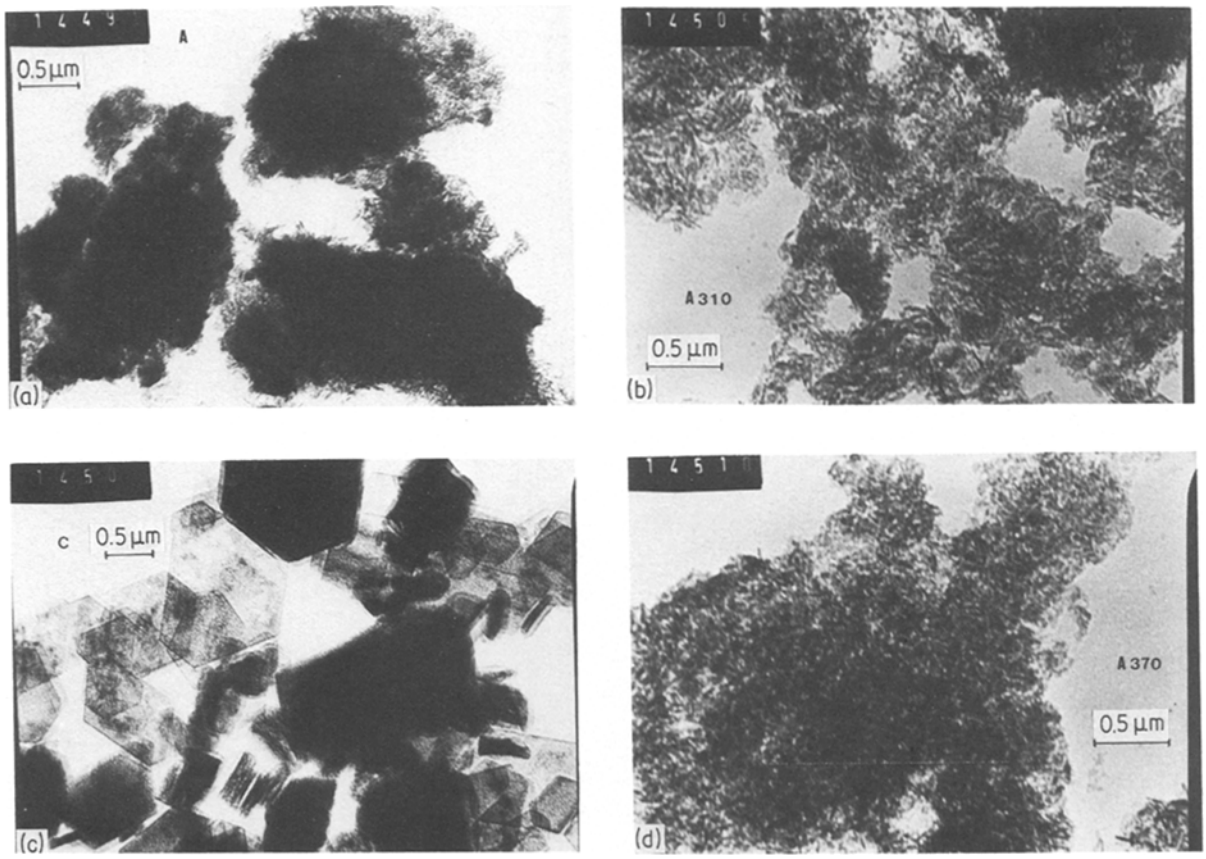

Figure 5 Electron micrographs of several selected samples.

explanation of the (A) exotherm in Fig. 1 based in the development of a recrystallization process in which the content of microstrains decreases giving place to an energy release should be considered. A similar phenomenon has been evidenced in other systems [23, 24] in which a notorious alteration of the structural parameters in the temperature interval in which an exothermal peak takes place has been considered as indicative. For $Ni(OH)_2$, the fact that the only sample in which the exotherm is detectable is that with a higher strain content (sample A) may be consistent with such an explanation. In this way, additional analyses of the X-ray diffraction line profiles were carried out for the samples prepared at the temperature immediately after the exotherm. As the most notable differences in strain content prior to the exotherm were observed in the [1 1 1] direction (see Table I), the analysis was developed for these reflections. These results are shown in Table I. The comparison of A310 and B370 with A370 and B340, respectively, shows that a decrease in microstrains content takes place, which is not accompanied by a sintering of crystallites. This behaviour may be indicative of the release of the energy stored as defects and may give new light on the nature of the exotherm.

References

1. R. B. FAHIM and A. I. ABU-SHADY, *J. Colloid Interface Sci.* **17** (1970) 10.
2. F. FIEVET and M. FIGLARZ, *J. Catal.* **39** (1975) 350.
3. C. L. CRONAN, F. J. MICALE, M. TOPIC, H. LEIDHEISER Jr, A. C. ZETTLEMOYER and S. POPOVIC, *J. Colloid Interface Sci.* **55** (1976) 546.
4. F. FIEVET, P. GERMI, F. DE BERGEVIN and M. FIGLARZ, *J. Appl. Cryst.* **12** (1979) 387.
5. C. L. CRONAN, F. J. MICALE, A. C. ZETTLEMOYER, M. TOPIC and H. LEIDHEISER Jr, *J. Colloid Interface Sci.* **75** (1980) 43.
6. J. J. BRACONIER, C. DELMAS, C. FOUASSIER, M. FIGLARZ, B. BEAUDOUIN and P. HAGENMULLER, *Rev. Chim. Minerale* **21** (1984) 496.
7. B. MANI and J. P. DE NEUFVILLE, *Mater. Res. Bull.* **19** (1984) 377.
8. D. J. COATES, J. W. EVANS and K. J. WESTMACOTT, *J. Mater. Sci.* **17** (1982) 3281.
9. V. SITAKARA RAO, S. RAJENDRAN and H. S. MAITI, *ibid.* **19** (1984) 3593.
10. E. Y. A. RODE, *Z. Neorg. Khim.* **1** (1956) 1430.
11. S. LE BIHAN and M. FIGLARZ, *Thermochim. Acta* **6** (1973) 319.
12. J. M. FERNANDEZ RODRIGUEZ, J. MORALES and J. L. TIRADO, *Surface Technol.* **26** (1985) 261.
13. J. MORALES and J. L. TIRADO, *Computers Chem.* **9** (1985) 7.
14. Th. H. DE KEIJSER, E. J. MITTEMEIJER and H. C. F. ROZENDAAL, *J. Appl. Cryst.* **16** (1983) 309.
15. J. MIGNOT and D. RONDOT, *Acta Crystallogr.* **A33** (1977) 327.
16. D. LOUER, D. WEIGEL and J. I. LANGFORD, *J. Appl. Cryst.* **5** (1972) 353.
17. S. LE BIHAN, J. GUENOT and M. FIGLARZ, *C.R. Acad. Sci.* **270C** (1970) 2131.
18. C. J. TOUSSAINT, *J. Appl. Cryst.* **4** (1971) 293.
19. G. MARTINEZ, J. MORALES and G. MUNUERA, *J. Colloid Interface Sci.* **81** (1981) 500.
20. R. GOMEZ VILLACIEROS, L. HERNAN, J. MORALES and J. L. TIRADO, *ibid.* **101** (1984) 392.
21. J. ROUQUEROL, F. ROUQUEROL, C. PERES, Y. GRILLET and M. BOUDELLAL, in "Characterization of Porous Solids" edited by S. J. Gregg, K. S. W. Sing and H. F. Stoeckli (Society Chemical Industry, London, 1979) p. 107.
22. G. MASON, *Proc. R. Soc.* **A390** (1983) 47.
23. J. MORALES, J. L. TIRADO and M. MACIAS, *J. Solid State Chem.* **53** (1984) 303.
24. C. BARRIGA, J. MORALES and J. L. TIRADO, *J. Mater. Sci.* **20** (1985) 941.

Received 28 October
and accepted 20 December 1985